Measuring nanomechanical motion with a microwave cavity interferometer

C. A. REGAL*, J. D. TEUFEL AND K. W. LEHNERT†

JILA, National Institute of Standards and Technology and the University of Colorado and Department of Physics, University of Colorado, Boulder, Colorado 80309, USA
*Current address: Norman Bridge Laboratory of Physics 12-33, California Institute of Technology, Pasadena, California 91125, USA
†e-mail: konrad.lehnert@jila.colorado.edu

Published online: 18 May 2008; doi:10.1038/nphys974

A mechanical resonator is a physicist's most tangible example of a harmonic oscillator. With the advent of micro and nanoscale mechanical resonators, researchers are rapidly progressing towards a tangible harmonic oscillator with motion that requires a quantum description. Challenges include freezing out the thermomechanical motion to leave only zero-point quantum fluctuations δx_{zp} and, equally importantly, realizing a Heisenberg-limited displacement detector. Here, we introduce a detector that can be in principle quantum limited and is also capable of efficiently coupling to the motion of small-mass, nanoscale objects, which have the most accessible zero-point motion. Specifically, we measure the displacement of a nanomechanical beam using a superconducting transmission-line microwave cavity. We realize excellent mechanical force sensitivity (3 aN Hz$^{-1/2}$), detect thermal motion at tens of millikelvin temperatures and achieve a displacement imprecision of 30 times the standard quantum limit.

As the imprecision of any detector is decreased to the level of zero-point motion, quantum measurement backaction will become an important source of displacement uncertainty. This backaction emerges to enforce the Heisenberg uncertainty principle, which for continuous displacement detection manifests as $\sqrt{S_x S_F} \geq \hbar$. Here, S_x and S_F are respectively the displacement-imprecision and backaction-force single-sided spectral densities[1]. In fact, at the minimum allowed total position uncertainty, referred to as the standard quantum limit (SQL), the measurement imprecision and the motion due to backaction must together contribute an uncertainty equal to the zero-point fluctuations.

A widely used displacement detector that, in principle, is capable of reaching the SQL is an optical cavity interferometer with a moving mirror[2]. Physically, at the SQL, our knowledge of the mirror position is limited equally by shot noise in the output signal and by motion of the mirror due to quantum fluctuations in the intracavity radiation pressure. This limit has long been of interest in quantum optics and in the gravitational wave detection community. Optical cavities generally outperform all other displacement detectors with regard to measurement imprecision; they can achieve shot-noise-limited position sensitivity as low as $\sim 10^{-19}$ m Hz$^{-1/2}$ (ref. 3). Still, reaching the SQL has historically been a challenge owing to the inaccessibility of quantum backaction effects[4,5]. Recent experimental progress using low-mass mirrored microcantilevers has made radiation pressure effects more observable[6–10].

However, the most successful approaches to the SQL so far have been electromechanical experiments. These experiments take place 'on-chip' in a dilution refrigerator, where thermomechanical motion is significantly reduced, and the mechanical objects are typically nanoscale and hence even less massive than microcantilevers. Examples include using a single-electron transistor[11,12] or an atomic point contact[13] for the displacement readout of a nanoscale flexural beam. Electromechanical experiments have revealed a displacement uncertainty less than 10 times the total uncertainty added by the measurement at the SQL and evidence for backaction[11,12]. Still, electromechanical experiments have not achieved the full quantum limit, typically owing to technical noise sources common to mesoscopic amplifiers.

Here, we present experiments that use the principles and advantages of an optical cavity interferometer with a moving mirror yet use 'light' at microwave frequencies. Operating at microwave frequencies enables us to also benefit from technology associated with electromechanical systems, such as low-mass mechanical objects and dilution-refrigerator temperatures. Specifically, we embed a nanomechanical flexural resonator inside a superconducting transmission-line microwave cavity, where the mechanical resonator's position couples to the cavity capacitance and thus to the cavity resonance frequency. Changes in this frequency can be sensitively monitored via homodyne detection of the phase shift of a microwave probe signal. Advantages of superconducting transmission-line cavities include large demonstrated quality factors ($Q > 10^5$) (ref. 14) and a tiny mode volume. In addition, the cavities are fabricated via a single deposition of a thin, superconducting film and thus are scalable as well as compatible with patterning of other nanoscale devices. These advantages have been leveraged in an array of other recent applications including microwave kinetic inductance detectors[14], achieving circuit quantum electrodynamics[15] and readout of superconducting quantum interference devices[16].

The analogy between our microwave system and an optical cavity interferometer is quite rigorous; the Hamiltonian describing both systems is

$$H = \hbar\omega_0\left(a^\dagger a + \frac{1}{2}\right) + \hbar\omega_m\left(b^\dagger b + \frac{1}{2}\right) - \hbar g a^\dagger a(b^\dagger + b)\delta x_{zp}, \quad (1)$$

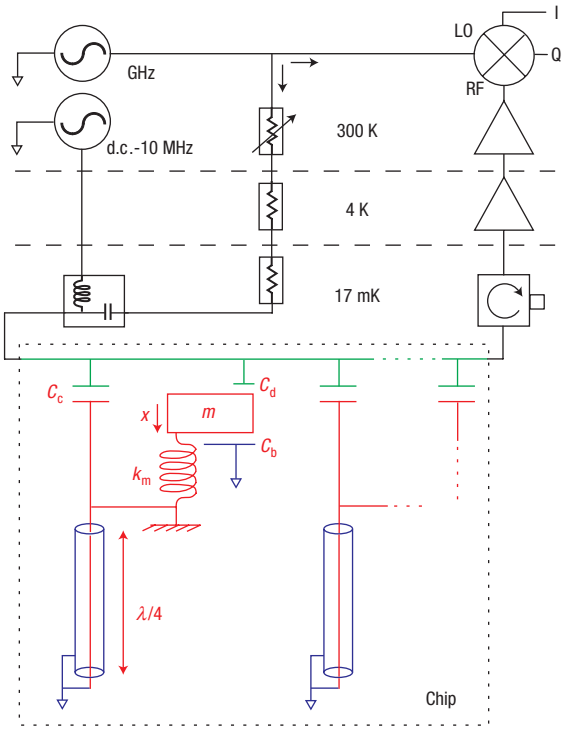

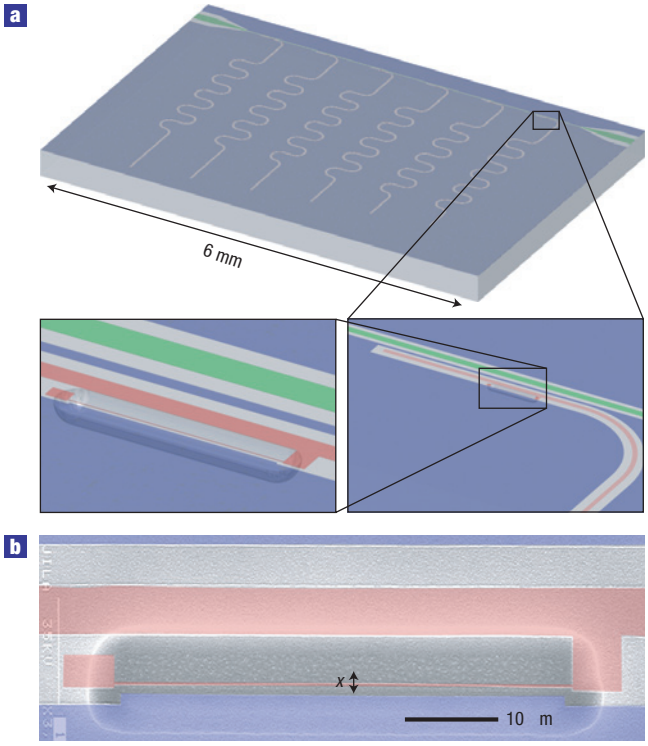

Figure 1 Measurement schematic diagram. Distributed microwave resonators (red and blue) with a line impedance of $Z_1 = 70\ \Omega$ are capacitively coupled, C_c, to a feedline (green). A nanomechanical beam (red) is coupled to each cavity via a capacitance C_b and to the feedline via C_d used for an electrostatic drive. The cavity coupling is characterized by 170 aF μm^{-1} and the drive coupling by 0.2 aF μm^{-1}. The beam motion is detected by measuring the phase shift of an injected microwave signal. This signal travels through the device and is then amplified first by a low-noise microwave HEMT amplifier and further at room temperature before going to the radiofrequency (RF) port of an inphase-quadrature (IQ) mixer. LO: local oscillator.

Figure 2 Illustration of our device geometry. a, The drawing shows frequency-multiplexed $\lambda/4$ microwave cavities; the lines are meandered to fit a quarter-wave on the chip. The cavity lines are formed from 5-μm-wide centre conductors separated from the ground plane by 10 μm slots. The lower panels zoom into a capacitive elbow coupler and a nanomechanical beam with the feedline shown in green, the ground plane in blue and the centre conductor in red. **b**, False-colour scanning electron microscope image of an embedded nanomechanical beam. This room-temperature image shows a top view of the beam, which is clamped on both ends and slightly bent owing to compressive stress (see the Methods section). An angled view of the same beam reveals that it is also bent out of the plane at its centre by 2.5 μm at room temperature. The area where the silicon was etched to release the beam appears as the darker oblong region.

where we have left out cavity and mechanical damping and driving terms. Here, the cavity and mechanical modes are described respectively by the operators a and b, ω_0 and ω_m are the bare resonant cavity and mechanical frequencies, and g is the effect of the displacement $\hat{x} = (b^\dagger + b)\delta x_{zp}$ on the perturbed cavity resonant frequency, ω_c. In both cases, the Heisenberg limit is enforced, as discussed above, by fluctuations in the optical or microwave field, that is, shot noise. Still, there are important practical differences between optical experiments and our microwave work. Although the optical shot-noise limit is achieved routinely, owing to the smaller photon energy of microwaves, measurement of microwave fields is currently dominated by amplifier noise. Nonetheless, microwave amplifier technology is progressing quickly, and in our experiments we use a commercially available high-electron-mobility transistor (HEMT) amplifier that already reaches a noise temperature of $k_b T_N/\hbar\omega_c = 30$ ($T_N = 7.5$ K). The small microwave photon energy also requires an excellent force sensitivity to detect quantum backaction, but our experiments aim to accommodate this requirement by going to the extremes of force sensitivity using floppy mechanical objects.

Our superconducting microwave cavities are formed from distributed transmission lines in a coplanar waveguide geometry and are patterned using an aluminium thin film on a high-purity silicon substrate. We use one-sided cavities that are shorted on one end and coupled to a 50 Ω feedline on the other end (Figs 1 and 2a); the cavity is overcoupled (dominated by external coupling not by internal losses) to minimize microwave power dissipation and signal loss. We study multiple cavities on a single chip by coupling six cavities to the feedline and address them individually via frequency multiplexing[14]. The quarter-wave resonances of our cavities are near $\omega_c = 2\pi \times 5$ GHz.

The nanomechanical objects we embed in the cavity are thin, high-aspect-ratio beams of conducting aluminium clamped on both ends (see the Methods section). We use a beam 50 μm long with a 100 nm by 130 nm cross-section (Fig. 2b). The thin beam gives us a small mass (an effective mass m of 2 pg), whereas the length provides both good coupling to the microwave cavity as well as a very small spring constant of a few millinewtons per metre. The beam is placed in the cavity such that the motion of its fundamental flexural mode changes the capacitance between the cavity centre conductor and the ground plane in a small section of the cavity (Fig. 2). To maximize the coupling, the gap between the beam and the ground plane is as small as is feasible (typically 1 μm), and the beam is embedded at a voltage antinode of the cavity standing wave. With the beam at this position, the cavity resonance frequency shifts according to

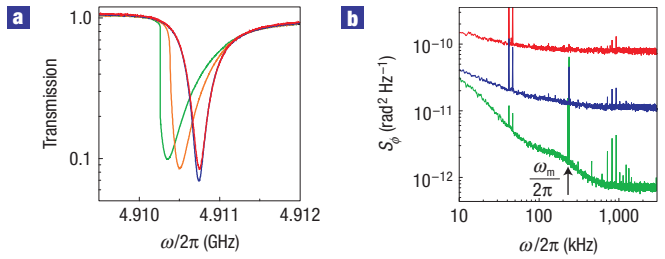

Figure 3 Microwave cavity characterization. a, Power transmission past the cavity normalized to transmission off resonance. The data are shown on a logarithmic scale for incident powers of 1,070 (green), 680 (orange), 68 (blue) and 11 (red) pW. All microwave powers quoted in this work have a 3 dB systematic uncertainty. At $P = 68$ pW, the quality factor of the resonance is $Q = (Q_{\mathrm{int}}^{-1} + Q_{\mathrm{ext}}^{-1})^{-1} = 10{,}000$. At the highest microwave powers, the resonance becomes nonlinear and eventually bistable when the superconducting critical current density is exceeded[36]. **b**, Measurement of the double-sideband cavity phase noise at incident powers of 1,070 (green), 68 (blue) and 11 (red) pW. The tone indicated with the black arrow can be attributed to the nanomechanical beam; the other tones are electronic in nature.

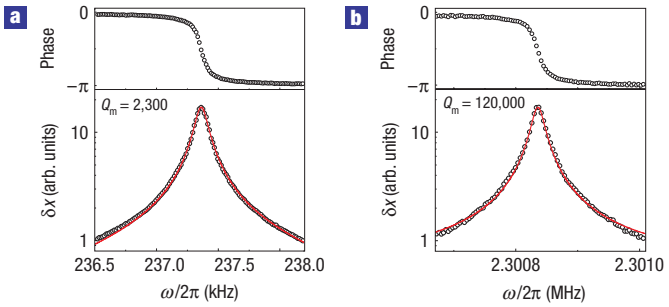

Figure 4 Resonant response of an aluminium nanomechanical beam to an electrostatic drive at $T_{\mathrm{cryo}} = 17$ mK. a, This experiment uses the beam shown in Fig. 2b, and we find $Q_{\mathrm{m}} = 2{,}300$. **b**, Response of a beam under tensile stress. Here, the resonance is near 2 MHz and the quality factor is greatly enhanced to $Q_{\mathrm{m}} = 120{,}000$. The predominant effect of the tensile stress is to change the stiffness while the dissipation, reflected by the resonant linewidth γ_{m}, remains approximately constant. The red lines are the square root of lorentzian fits to the data.

$(1/\omega_{\mathrm{c}})(\partial\omega_{\mathrm{c}}/\partial x) = -(\partial C_{\mathrm{b}}/\partial x)4Z_1\omega_{\mathrm{c}}/2\pi$ for a $\lambda/4$ cavity, where $\partial C_{\mathrm{b}}/\partial x$ is the effect of the beam motion on the cavity capacitance and $-\partial\omega_{\mathrm{c}}/\partial x$ is the coupling g of equation (1).

To detect nanomechanical motion with our microwave cavity interferometer, we inject a microwave tone near a cavity resonance and monitor the phase of the transmitted signal; this phase directly reflects the cavity resonance frequency and hence the beam displacement as described above. Figure 1 shows how we extract the phase (Q) and amplitude (I) quadratures of the transmitted signal using a homodyne detection scheme.

Figure 3a shows the microwave cavity resonant response. Here, we measure the relative transmission past the cavity for a set of incident microwave powers P at a dilution-refrigerator temperature of 17 mK, far below the 1.2 K critical temperature of aluminium. At low microwave power, the resonant behaviour is characterized by unity transmission off resonance and by a lorentzian response that dips to a value determined by the intracavity losses compared with the feedline coupling. Our imprecision in the nanomechanical beam position readout is determined by fluctuations in the associated dispersive phase signal on resonance. Figure 3b shows our experimentally observed cavity phase fluctuations as the spectral density S_ϕ. At the highest response frequencies, we see a phase noise consistent with the HEMT amplifier noise, whereas at lower frequencies, the phase noise is enhanced. This extra noise has recently been traced to two-level fluctuators in the silicon substrate[17].

An important feature of our experiment is the ability to actuate the mechanical beam using an electrostatic drive. This method avoids the problematic aspects of magnetomotive driving such as large currents in the beam and applied magnetic fields that are incompatible with high-Q superconducting cavities[18]. In our device, we incorporate a small capacitive coupling between the beam and the microwave feedline, which enables us to electrostatically drive the beam by coupling low-frequency signals onto the feedline (Fig. 1). Using a bias-tee, we introduce an a.c. signal near the ω_{m} and a d.c. voltage resulting in an electrostatic force $F_{\mathrm{el}}(\omega) = V_{\mathrm{d.c.}}V_{\mathrm{a.c.}}(\omega)(\partial C_{\mathrm{d}}/\partial x)$, where C_{d} is the drive capacitance between the feedline and the beam. To assure that the effect of the beam motion remains in the phase quadrature of the microwave signal, we design C_{d} to be much smaller than C_{b}.

Figure 4a demonstrates nanomechanical displacement detection using our microwave cavity interferometer. Here, the beam motion we are measuring is the response of the beam shown in Fig. 2b to an electrostatic drive. We see a clean response on a logarithmic scale, the expected π phase shift and good agreement with the anticipated lorentzian response (red line) of our high-Q resonance. We measure a quality factor of $Q_{\mathrm{m}} = 2{,}300$ and find the mechanical resonance at $\omega_{\mathrm{m}} = 2\pi \times 237$ kHz; this frequency is near our expectation for a tension-free beam with our geometry.

Figure 4b demonstrates the mechanical response we observe using a 50-μm-long beam fabricated from an aluminium film under tensile stress (see the Methods section). The stress significantly increases ω_{m} to near $2\pi \times 2.3$ MHz and Q_{m} to 120,000. This quality factor is surprisingly, yet pleasingly, large for a beam fabricated from an amorphous metal and of this surface-to-volume ratio[19–21]. When working with mechanical objects with ω_{m} in the megahertz regime, we must take into account that the sidebands generated by the beam's motion move outside the cavity bandwidth, $\gamma_{\mathrm{c}} = \omega_{\mathrm{c}}/Q = 2\pi \times 490$ kHz. In this so-called good-cavity limit, to acquire the response seen in Fig. 4b, we detune the injected microwave signal off resonance by ω_{m} to place one of the sidebands on the cavity resonance.

The focus of this article will be on characterizing our detector using the few-hundred-kilohertz mechanical resonance of Fig. 4a and an injected microwave tone tuned to the cavity resonance. Here, in the so-called bad-cavity limit, our microwave interferometer faithfully reproduces the position of the beam. Our first goal was to detect the thermally driven displacement fluctuations of our beam at dilution-refrigerator temperatures, which for our high-Q mechanical resonators are given by

$$S_x(\Delta\omega_{\mathrm{m}}) = \frac{1}{(m\omega_{\mathrm{m}}\gamma_{\mathrm{m}})^2}\frac{4m\gamma_{\mathrm{m}}k_{\mathrm{b}}T}{1+4\Delta\omega_{\mathrm{m}}^2/\gamma_{\mathrm{m}}^2},$$

where $\gamma_{\mathrm{m}} = \omega_{\mathrm{m}}/Q_{\mathrm{m}}$, $\Delta\omega_{\mathrm{m}} = \omega - \omega_{\mathrm{m}}$ and T is the bath temperature. The inset to Fig. 5 shows the observed displacement fluctuations, with no intentional beam driving, at three different values of the dilution-refrigerator temperature T_{cryo}. The white-noise background is the imprecision S_x^{im}, whereas the height of the peak above the background describes the real fluctuations in the beam position. To understand the temperature-dependent response (and to calibrate the beam-to-cavity coupling), in Fig. 5

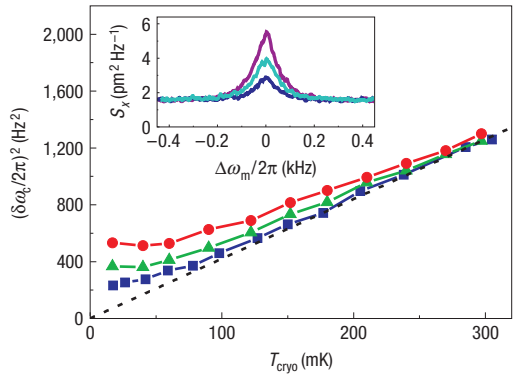

Figure 5 Integrated mechanical beam fluctuations in units of cavity resonance frequency shift $\delta\omega_c$. The three data sets correspond to $P = 4$ pW (blue squares), 27 pW (green triangles) and 68 pW (red circles). The dashed line shows the linear fit described in the text from which we extract the coupling g. Inset: Examples of the lorentzian response (near $\omega_m = 2\pi \times 237$ kHz) for dilution-refrigerator temperatures of 210 mK, 122 mK and 40 mK at $P = 11$ pW.

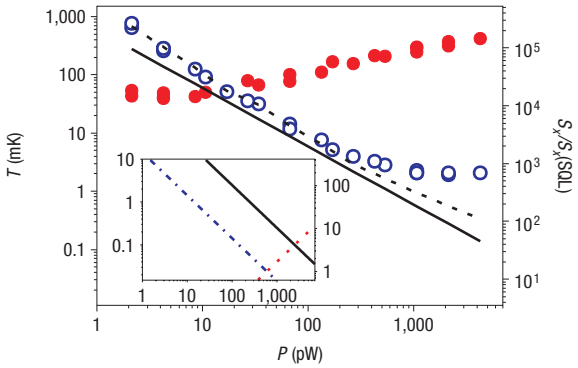

Figure 6 Imprecision temperature (blue open circles) and saturation temperature (red circles) as a function of incident microwave power. The lines represent the expected imprecision due to our current microwave amplifier ($T_N = 7.5$ K); the dashed line includes the loss of microwave power in the cavity, whereas the solid line represents the expectation for a lossless cavity. The right vertical axis shows the position uncertainty in units of S_x(SQL). Inset: Over the same range of power, we calculate the quantum limit of displacement detection for the optimized parameters quoted in the text. The lines correspond to the shot-noise limit (dashed–dotted line), the quantum backaction (dotted line) and the imprecision due to a $T_N = 5$ K voltage amplifier (solid line).

we examine the integrated signal under the lorentzian as a function of T_{cryo} for a set of incident microwave powers P. In an ideal system, the integrated response should depend linearly on the temperature according to $\delta\omega_c^2 = (g^2 k_b / m\omega_m^2)(T_{cryo} + T_{ba})$, where $T_{ba} = S_F^{ba}/4k_b m\gamma_m$ is the equivalent backaction temperature. If we focus on the lowest microwave power results (blue squares) and the highest dilution-refrigerator temperatures, we see that the response is linear down to ∼100 mK. Here, linear fits reveal that the backaction is small compared with relevant uncertainties, and we extract a coupling of $g = 2\pi \times 1.16$ kHz nm^{-1} using points above 127 mK (dashed line). This value of g corresponds to a capacitance change of $\partial C_b/\partial x = 170$ aF μm^{-1}, which is consistent with our numerically calculated expectation.

At lower values of T_{cryo} and higher microwave powers (green triangles and red circles), the beam temperature decouples from T_{cryo} leading to a saturation behaviour. The nonlinear behaviour can be explained by a deterioration of the thermal link between the beam and the refrigerator at low temperatures in the presence of a temperature-independent heat load on the beam. The microwave power dependence of the magnitude of the effect suggests that the origin of the heat load is microwave power dissipation. Whereas an ideal, fully overcoupled device would dissipate no microwave power on-chip, in our current device, because our external quality factor of $Q_{ext} = 14{,}000$ is not much smaller than our internal quality factor $Q_{int} = 38{,}000$, we dissipate power of the order of picowatts. We have made an initial investigation into the mechanism by which the microwave dissipation results in beam heating. By using a different cavity on the same chip as a crude thermometer, we know that the dissipated power does not heat the entire chip above T_{cryo}. Hence, the heating must be a more local effect, but further experiments are required to determine its full origin. Note that classical amplitude or phase noise in the microwave drive could be another source of heating, but we can rule out this mechanism because fluctuations large enough to cause significant heating would be easily observed above the noise level of our microwave amplifier.

The results in Fig. 5 provide valuable information about our ability to extract quantum backaction with our device. With a well-understood and controllable bath temperature and precise measurements, it is possible to detect very small equivalent backaction temperatures $T_{ba} < T_{cryo}$ with a linear extrapolation to zero temperature. In our case, the nonlinear dependence of the beam fluctuations on T_{cryo} represents our largest limitation to extracting T_{ba}. Thus, as a conservative upper limit to T_{ba}, we report the equivalent temperature our beam fluctuations saturate to at $T_{cryo} = 17$ mK, which we will refer to as T_{sat}. Figure 6 shows T_{sat} along with the imprecision temperature $T_{im} = S_x^{im} m\omega_m^2 \gamma_m / 4k_b$ as a function of P. At the lowest powers, the imprecision dominates over the beam fluctuations. As the power is increased, the imprecision drops linearly with power as expected, but at the highest microwave powers, it is enhanced by cavity phase noise to a value above our microwave amplifier noise floor (dashed line).

From the results in Fig. 6, we can assess how close an approach we have made to the SQL. The minimum uncertainty in continuous position detection at the Heisenberg limit $S_x^{im} S_F^{ba} = \hbar^2$ occurs at the point where $S_x^{im} = S_x^{ba} = S_F^{ba}/(m\omega_m\gamma_m)^2$. Here, the imprecision and the backaction both contribute $S_x(\mathrm{SQL}) = \hbar/m\omega_m\gamma_m$. We can convert the imprecision and saturation temperatures in Fig. 6 into a position spectral density compared with this minimum value via $S_x/S_x(\mathrm{SQL}) = 4k_b T/\hbar\omega_m$. This result is shown on the right axis of Fig. 6. Our limit on the imprecision alone at the highest microwave powers corresponds to, in linear units, $30\sqrt{S_x(\mathrm{SQL})}$. The total minimum position uncertainty we achieve occurs at $P = 20$ pW and is given by $\sqrt{S_x^{tot}} = 130\sqrt{S_x^{tot}(\mathrm{SQL})}$, where to be explicit S_x^{tot} here is $S_x^{im} + S_x^{sat}$, which is an upper bound on our ability to measure $S_x^{im} + S_x^{ba}$.

We can also extract absolute values for the achieved sensitivity. Our imprecision is limited to 200 fm Hz$^{-1/2}$ at the highest microwave powers, which is a modest achievement compared with optical systems[3]. On the other hand, our total force sensitivity, $\sqrt{S_F^{tot}} = \sqrt{4k_b(T_{im} + T_{sat})m\gamma_m}$, is 3 aN Hz$^{-1/2}$ at $P = 20$ pW. This value is near the record mechanical force sensitivity of 0.8 aN Hz$^{-1/2}$ achieved using a fibre-optic interferometer and a silicon cantilever[22].

To closer approach the SQL with our microwave cavity interferometer, the foremost task will be to decrease the dissipation that leads to a finite T_{sat} by using devices with a larger Q_{int}. Another route to improvement is to increase ω_m, which will decrease thermal fluctuations and the dissipative force compared

with quantum fluctuations, as well as decrease the $\nu^{-1/2}$ cavity phase noise. However, to maintain the force sensitivity, an increase in the mechanical spring constant should be accompanied by an increase in the beam-to-cavity coupling g. One option for increasing g would be to decrease the total cavity capacitance by operating at larger ω_c or by using a higher-impedance microwave cavity or lumped-element circuit.

It is instructive to assess what we could achieve in future experiments using optimized, yet likely realizable, parameters. Consider a device described by $\omega_m = 2\pi \times 2\,\mathrm{MHz}$, $m = 2\,\mathrm{pg}$, $Q_m = 100{,}000$, $\omega_c = 2\pi \times 12\,\mathrm{Hz}$, $Q_{int} \gg Q_{ext} = 3{,}000$ and $g = 2\pi \times 20\,\mathrm{kHz\,nm^{-1}}$. Furthermore, assume we modify our geometry to measure in reflection off of a single-sided cavity with a single port. For this more ideal geometry and a microwave probe at ω_c, the quantum-limited imprecision expected for detection via a square-law detector would be the shot-noise limit

$$S_x^{sn} = \frac{\hbar\omega_c(1+4(\omega_m/\gamma_c)^2)}{2(g/\omega_c)^2 P(4Q)^2},$$

and correspondingly $S_F^{ba} = \hbar^2/S_x^{sn}$. Our calculated expectation for S_x^{sn} and S_F^{ba} is shown in the inset to Fig. 6 and overall presents a promising picture in which the SQL would occur at a realizable power of 600 pW. Even with the added noise of a $T_N = 5\,\mathrm{K}$ HEMT amplifier (solid line), the minimum uncertainty point, assuming ideal backaction, would be a factor of two above the SQL in linear units. A future goal will be to incorporate even better microwave amplifiers that could soon be available given recent interest in developing novel microwave amplifiers near the quantum limit[23–25]. However, even a quantum-limited voltage amplifier measuring both field quadratures will result in an imprecision a factor of two above the shot-noise limit[26], and to fully reach the SQL, an amplifier that detects only one quadrature must be used.

An advantage of our device is that in addition to being a simple, yet promising detector, it presents a natural platform for manipulation and cooling of mechanical motion. Possibilities include active feedback cooling, or 'cold damping', using our ability to apply electrostatic forces as well as passive cooling based on radiation pressure. With the availability of these complementary cooling techniques, we are well poised to attempt targeted cooling of a mechanical mode below the tens of millikelvin temperatures already achieved with our refrigerator[27,28], a task that has proved difficult in single-electron transistor devices[11,12].

Of particular interest is the possibility of passive cooling using radiation pressure in the good-cavity limit that we have demonstrated here. As first explored by Braginsky[29], dynamical backaction due to radiation pressure can lead to a passive cooling or amplification of the mechanical motion when the injected tone is detuned from the cavity resonance. These effects have recently been observed in optical cavities with micromechanical mirrors[6–10] and radiofrequency circuits[30] and have been suggested as a method of cooling and manipulating a beam coupled to a transmission-line cavity[31,32]. In the good-cavity limit, the cooling mechanism becomes analogous to resolved sideband cooling of trapped ions[33] and in principle, in this regime, it is possible to cool fully to the mechanical ground state[34,35].

METHODS

The device is fabricated using a combination of electron-beam lithography and photolithography, and the beam and cavity are formed from the same thermally evaporated aluminium film in a single lift-off process. The beam is patterned directly on the silicon substrate and suspended at the end of the process with an isotropic, dry silicon etch. A relatively deep etch of 4 μm is typically required to release our mechanical beams with low spring constants. An insulating layer of SiO_2 underneath the rest of the pattern is used to protect the coplanar waveguide slots during the etch.

Our initial thermally evaporated aluminium film contains significant compressive stress. To adjust the stress of the aluminium beam, we partially anneal the device at 150–350 °C in atmosphere before releasing the beam from the substrate. The final stress of the beam at cryogenic temperatures is affected by the differential thermal coefficient of expansion of silicon and amorphous aluminium. We estimate that between room and cryogenic temperatures, the aluminium film shrinks by a few tenths of a per cent compared with its clamping locations. Hence, the beam in Fig. 4a has significant compressive stress at room temperature (Fig. 2b) but less compressive stress at T_{cryo}; the beam in Fig. 4b has little stress at room temperature but significant tensile stress at T_{cryo}.

As our inphase-quadrature mixer (Marki IQ03076XP) has orthogonal outputs near 5 GHz, we can place all of the phase information in the Q channel simply by rotating the phase of the signal into the local oscillator of the mixer. The voltage fluctuations measured in the Q quadrature S_V^Q are then all that is required to extract the integrated cavity resonance frequency shift plotted in Fig. 5. The relationship between the cavity resonance frequency fluctuations and the voltage fluctuations is

$$S_{\omega_c} = \frac{\omega_c^2(1+4(\omega_m/\gamma_c)^2)}{(2Q)^2 V_0^2(1-S_{min})^2} S_V^Q,$$

where V_0 is the voltage amplitude of the transmission off resonance and S_{min} is the normalized transmission past the cavity on resonance. The term $1+4(\omega_m/\gamma_c)^2$ accounts for filtering of the cavity response at ω_m and goes to unity in the bad-cavity limit. The integrated response in units of cavity resonance frequency shift is then given by $\delta\omega_c^2 = S_{\omega_c}^0 \gamma_m/4$, where $S_{\omega_c}^0$ is the magnitude of the lorentzian response at $\Delta\omega_m = 0$. The temperature dependence of the Q, S_{min} and Q_m must be taken into account in these conversions, but we restrict our measurements to below 300 mK, where the values change by less than ∼20%.

In Fig. 6, we extend our measurement into the regime where the cavity resonance becomes nonlinear (Fig. 3a) and hence conversion between S_V^Q and S_{ω_c} becomes less straightforward to calculate. To extract this conversion at nonlinear microwave powers, we carry out a separate calibration experiment in which we apply a constant electrostatic drive and compare the beam response at high microwave power with the known response at low power.

Received 14 January 2008; accepted 15 April 2008; published 18 May 2008.

References

1. Clerk, A. A. Quantum-limited position detection and amplification: A linear response perspective. *Phys. Rev. B* **70**, 245306 (2004).
2. Caves, C. M. Quantum-mechanical noise in an interferometer. *Phys. Rev. D* **23**, 1693–1708 (1981).
3. Arcizet, O. *et al.* High-sensitivity optical monitoring of a micromechanical resonator with a quantum-limited optomechanical sensor. *Phys. Rev. Lett.* **97**, 133601 (2006).
4. Tittonen, I. *et al.* Interferometric measurements of the position of a macroscopic body: Towards observation of quantum limits. *Phys. Rev. A* **59**, 1038–1044 (1999).
5. Braginsky, V. B. *Systems With Small Dissipation* (Univ. of Chicago Press, Chicago, 1985).
6. Arcizet, O., Cohadon, P.-F., Briant, T., Pinard, M. & Heidmann, A. Radiation-pressure cooling and optomechanical instability of a micromirror. *Nature* **444**, 71–74 (2006).
7. Gigan, S. *et al.* Self-cooling of a micromirror by radiation pressure. *Nature* **444**, 67–70 (2006).
8. Kleckner, D. & Bouwmeester, D. Sub-kelvin optical cooling of a micromechanical resonator. *Nature* **444**, 75–78 (2006).
9. Schliesser, A., Del'Haye, P., Nooshi, N., Vahala, K. J. & Kippenberg, T. J. Radiation pressure cooling of a micromechanical oscillator using dynamical backaction. *Phys. Rev. Lett.* **97**, 243905 (2006).
10. Thompson, J. D. *et al.* Strong dispersive coupling of a high finesse cavity to a micromechanical membrane. *Nature* **452**, 72–75 (2008).
11. LeHaye, M. D., Buu, O., Camarota, B. & Schwab, K. C. Approaching the quantum limit of a nanomechanical resonator. *Science* **304**, 74–77 (2004).
12. Naik, A. *et al.* Cooling a nanomechanical resonator with quantum back-action. *Nature* **443**, 193–196 (2006).
13. Flowers-Jacobs, N. E., Schmidt, D. R. & Lehnert, K. W. Intrinsic noise properties of atomic point contact displacement detectors. *Phys. Rev. Lett.* **98**, 096804 (2007).
14. Day, P. K., LeDuc, H. G., Mazin, B. A., Vayonakis, A. & Zmuidzinas, J. A broadband superconducting detector suitable for use in large arrays. *Nature* **45**, 817–821 (2003).
15. Wallraff, A. *et al.* Circuit quantum electrodynamics: Coherent coupling of a single photon to a Cooper pair box. *Nature* **431**, 162–167 (2004).
16. Mates, J. A. B., Hilton, G. C., Irwin, K. D. & Vale, L. R. Demonstration of a multiplexer of dissipationless superconducting quantum interference devices. *Appl. Phys. Lett.* **92**, 023514 (2008).
17. Gao, J., Zmuidzinas, J., Mazin, B. A., LeDuc, H. G. & Day, P. K. Noise properties of superconducting lithographed microwave resonators. *Appl. Phys. Lett.* **90**, 102507 (2007).
18. Frunzio, L., Wallraff, A., Schuster, D., Majer, J. & Schoelkopf, R. Fabrication and characterization of superconducting circuit QED devices for quantum computation. *IEEE Trans. Appl. Supercond.* **15**, 860–863 (2005).
19. Ekinci, K. L. & Roukes, M. L. Nanoelectromechanical systems. *Rev. Sci. Instrum.* **76**, 061101 (2005).
20. Verbridge, S. S., Parpia, J. M., Reichenbach, R. B., Bellan, L. M. & Craighead, H. G. High quality factor resonance at room temperature with nanostrings under high tensile stress. *J. Appl. Phys.* **99**, 124304 (2006).
21. Zwickl, B. M. *et al.* High quality mechanical and optical properties of commercial silicon nitride membranes. *Appl. Phys. Lett.* **92**, 103125 (2008).

22. Mamin, H. J. & Rugar, D. Sub-attonewton force detection at millikelvin temperatures. *Appl. Phys. Lett.* **79**, 3358–3360 (2001).
23. Yurke, B. *et al.* Observation of parametric amplification and deamplification in a Josephson parametric amplifier. *Phys. Rev. A* **39**, 2519–2533 (1989).
24. Muck, M., Kycia, J. B. & Clarke, J. Superconducting quantum interference device as a near-quantum-limited amplifier at 0.5 GHz. *Appl. Phys. Lett.* **78**, 967–969 (2001).
25. Castellanos-Beltran, M. A. & Lehnert, K. W. Widely tunable parametric amplifier based on a superconducting quantum interference device array resonator. *Appl. Phys. Lett.* **91**, 083509 (2007).
26. Caves, C. M. Quantum limits on noise in linear amplifiers. *Phys. Rev. D* **26**, 1817–1839 (1982).
27. Genes, C., Vitali, D., Tombesi, P., Gigan, S. & Aspelmeyer, M. Ground-state cooling of a micromechanical oscillator: Comparing cold-damping and cavity-assisted cooling schemes. *Phys. Rev. A* **77**, 033804 (2008).
28. Poggio, M., Degen, C. L., Mamin, H. J. & Rugar, D. Feedback cooling of a cantilever's fundamental mode below 5 mK. *Phys. Rev. Lett.* **99**, 017201 (2007).
29. Braginsky, V. B. & Manukin, A. B. *Measurement of Weak Forces in Physics Experiments* (The Univ. of Chicago Press, Chicago, 1977).
30. Brown, K. R. *et al.* Passive cooling of a micromechanical oscillator with a resonant electric circuit. *Phys. Rev. Lett.* **99**, 137205 (2007).
31. Xue, F., Wang, Y. D., Liu, Y. & Nori, F. Cooling a micro-mechanical beam by coupling it to a transmission line. *Phys. Rev. B* **76**, 205302 (2007).
32. Vitali, D., Tombesi, P., Woolley, M. J., Doherty, A. C. & Milburn, G. J. Entangling a nanomechanical resonator and a superconducting microwave cavity. *Phys. Rev. A* **76**, 042336 (2007).
33. Wineland, D. J. & Itano, W. M. Laser cooling of atoms. *Phys. Rev. A* **20**, 1521–1540 (1979).
34. Marquardt, F., Chen, J. P., Clerk, A. A. & Girvin, S. M. Quantum theory of cavity-assisted sideband cooling of mechanical motion. *Phys. Rev. Lett.* **99**, 093902 (2007).
35. Wilson-Rae, I., Nooshi, N., Zwerger, W. & Kippenberg, T. J. Theory of ground state cooling of a mechanical oscillator using dynamical backaction. *Phys. Rev. Lett.* **99**, 093901 (2007).
36. Dahm, T. & Scalapino, D. J. Theory of intermodulation in a superconducting microstrip resonator. *J. Appl. Phys.* **81**, 2002–2009 (1997).

Acknowledgements

We acknowledge support from the National Science Foundation's Physics Frontier Center for Atomic, Molecular and Optical Physics and from the National Institute of Standards and Technology; C.A.R. acknowledges support from the Fannie and John Hertz Foundation. The authors acknowledge R. J. Schoelkopf, S. M. Girvin, K. D. Irwin, D. Alchenberger, M. A. Castellanos-Beltran and N. E. Flowers-Jacobs for enlightening conversations and technical assistance.

Author information

Reprints and permission information is available online at http://npg.nature.com/reprintsandpermissions. Correspondence and requests for materials should be addressed to K.W.L.